Improvement of liquid crystal tunable lenses with weakly conductive layers using multi-frequency driving

TOM VANACKERE[1,*], TOM VANDEKERCKHOVE[1], ELKE CLAEYS[1], JOHN PUTHENPARAMPIL GEORGE[1], KRISTIAAN NEYTS[1], AND JEROEN BEECKMAN[1,**]

[1] Department of Electronics & Information Systems, Ghent University, Technologiepark-Zwijnaarde 126, 9052 Ghent, Belgium
[*] Now at Department of Information Technology, Ghent University, Technologiepark-Zwijnaarde 126, 9052 Ghent, Belgium
[**] Corresponding author: jeroen.beeckman@ugent.be

Compiled January 14, 2020

A common technique to realize the gradient electric field profile that is required in liquid crystal tunable lenses is the use of a weakly conductive layer. Thanks to this layer, an applied voltage with a certain frequency allows to obtain a refractive index profile that is required for the lens operation. Due to the limited degrees of freedom however, it is not possible to avoid aberrations in a weakly conductive layer based tunable lens for a continuously tunable focal length. In this work, we discuss the use of additional higher frequency components in the voltage signal to reduce the lens aberrations drastically.

http://dx.doi.org/10.1364/ao.XX.XXXXXX

1. INTRODUCTION

Liquid Crystals (LCs) possess properties of both crystalline and fluid materials. The electric permittivity and refractive index of LCs are strongly dependent on the orientation of the director, which is the local average orientation of the LC molecules. With an applied quasi-static electric field, it is possible to change the optical properties of the LC. This is commonly used in Liquid Crystal Displays (LCDs) but also in beam steering devices [1, 2], spatial light modulators [3, 4] and tunable lenses [5]. Lenses with an electrically tunable focal distance are often useful when mechanical focusing is difficult. Lens operation requires a spatially varying Optical Path Length (OPL) to change the phase profile of the light and focus it. For LC devices with a constant thickness this means that the electric field over the LC layer needs to be non-uniform. Multiple designs for tunable lenses based on LCs have previously been proposed, such as the one with an optically hidden dielectric layer [6]. Some of them work with several electrodes that need to be individually addressed [7–9]. Depending on the design, the number of electrodes can be quite high and the distance between the electrodes small to ensure an appropriate OPL profile over the lens diameter. Another type of LC lens uses weakly conductive materials to ensure a monotonic variation in the electric potential [10–13]. A simple design is to use only two electrodes where one is a circular addressing electrode combined with a weakly conductive layer. This reduces the amount of required wires and removes diffraction due to the multiple addressing electrodes. It however also reduces the number of voltages that can be applied to control the electric field steering of the LC. While all LC devices require an AC driving voltage to avoid ion drift and charge build up [14, 15], LC devices using conductive layers need to pay special attention to the driving frequency since it influences the distance over which the potential drops over the weakly conductive layer. The sheet resistance of the weakly conductive layer and the driving frequency need to be matched in order to have the required voltage drop in the radial direction [16]. In principle, there are only two ways to change the behavior of the lens, which is the amplitude and the frequency of the applied voltage. For lenses with a continuously variable focus, it is impossible to obtain the desired optical parabolic phase profile for every possible focal strength. Consequently, the lens exhibits strong aberration which cannot be compensated [16]. A possible way to reduce the aberrations is to add an additional ring of highly conductive material inside the hole [17–20], but again, this technique cannot reduce the aberrations for every possible focal length. Here we propose a novel way of aberration compensation by including additional degrees of freedom into the driving of the liquid crystal lens. By using multiple frequency components in the voltage signal, the OPL profile can be optimized and aberrations can be strongly reduced.

2. THEORETICAL BACKGROUND

Consider a liquid crystal lens that consists of a LC layer that is sandwiched between two conductive layers as depicted in figure 1. The bottom conductive layer has an infinite sheet conductivity, while the top layer consists of two parts: a circular area of radius R with finite sheet conductivity σ_s and a surrounding area with infinite σ_s. The anisotropic permittivity of the LC is denoted as $\bar{\bar{\varepsilon}}(x, y, z)$ and can be calculated from the local director orientation.The director orientation is in turn depending on the electric fields, which results in two differential equations to be solved simultaneously. To simulate the LC lens, an approximate model is used to significantly reduce the complexity of the problem as in [16]. The initial three dimensional case is reduced to a two dimensional one by introducing an effective permittivity $\varepsilon_{\text{eff}}(x, y)$ that is independent of z. This is a good

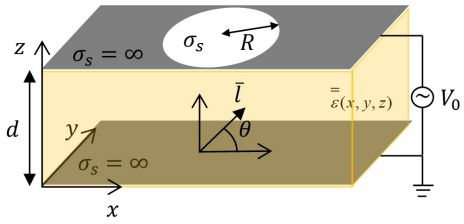

Fig. 1. Schematic view of a liquid crystal lens with a circular weakly conductive layer.

approximation when the radius of the weakly conductive material is much larger than the LC layer thickness, which is true in most of the lenses demonstrated using this principle. In case the LC layer has antiparallel alignment along the x direction, then the director $\bar{l}$ can be described using the inclination angle θ as $l_x = \cos\theta$, $l_y = 0$ and $l_z = \sin\theta$. The distribution of θ along the z axis can be calculated based on the local voltage between the top and bottom conductive layers. The permittivity is then written as $\varepsilon_{i,j} = \delta_{i,j}\varepsilon_\perp + \Delta\varepsilon l_i l_j$ with l_i the components of the director along x, y and z, $\varepsilon_\perp$ the permittivity of the LC perpendicular to the director and $\Delta\varepsilon$ the dielectric anisotropy of the LC. The bottom layer is grounded, so the potential V at the top layer fully determines the behavior of the system. The surface current density $\bar{K}$ in the weakly conductive layer can be written as $\bar{K} = -\sigma_s \nabla_\perp V$. The gradient only contains derivatives in the plane of the layer. As the LC layer acts as a capacitance, the current density between the two electrodes can be written as $J_z = \frac{\varepsilon_{\text{eff}}}{d}\frac{\partial V}{\partial t}$, with d the thickness of the LC layer.

These two equations are connected via the conservation of charge $\nabla_\perp \cdot \bar{K} = -J_z$. This results in the following differential equation

$$\nabla_\perp^2 V = -\frac{\varepsilon_{\text{eff}}}{d\sigma_s}\frac{\partial V}{\partial t} \tag{1}$$

It is important to remember that ε_{eff} depends on the electric field and thus on V, making this a nonlinear differential equation. Taking advantage of the circular design of the lens, cylindrical coordinates can be used to further reduce the dimensions of the problem. By writing the Laplacian operator in cylindrical coordinates, the equation becomes

$$\frac{\partial^2 V}{\partial r^2} + \frac{1}{r}\frac{\partial V}{\partial r} + \frac{1}{r^2}\frac{\partial^2 V}{\partial \varphi^2} + \frac{\varepsilon_{\text{eff}}}{d\sigma_s}\frac{\partial V}{\partial t} = 0 \tag{2}$$

In the frequency domain, the partial differential equation is easily obtained by replacing $\partial/\partial t$ by $j\omega$. Because of the circular symmetry, the derivative to φ is zero, making sure the problem becomes one dimensional. The resulting problem can be solved numerically using a nonlinear differential equation solver. An initial guess is required, for which the equation is solved analytically in case of a constant effective permittivity. In this case the solution is a zeroth order Bessel function of the first kind. If the applied voltage is sinusoidal with amplitude V_0 and an angular frequency ω, the distribution becomes:

$$V(r) = V_0 \frac{J_0(ar)}{J_0(aR)}, \text{ where } a = \frac{1-j}{\sqrt{\omega\varepsilon_{\text{eff}}/\sigma d}} \tag{3}$$

Figure 2(a) shows the effective permittivity ε_{eff} and the effective refractive index n_{eff} (being the OPL divided by the LC layer thickness d) as a function of voltage. Figure 2(b) shows the resulting n_{eff} as a function of the normalized radial coordinate r/R for an applied voltage of 5 V and three different frequencies. For the parameters of this calculation, the properties of the LC E7 (Merck) are used. The radius of the lens is $R = 1$ mm, the sheet resistance $\sigma_s = 0.5$ GΩ/sq and the LC layer thickness $d = 10$ μm. The value of n_{eff} is obtained by solving the nonlinear partial differential equation (2) and by converting the resulting variation of V into an effective refractive index profile. It is clear from this figure that lower driving frequencies result in an increased voltage towards the center, while higher driving frequencies only influence the LC behavior in the outer regions of the lens. Ideally, the OPL is parabolic across the diameter. To assess the quality of the OPL, a linear combination of the first four circularly symmetric Zernike Polynomials $Z_0^0(\rho) = a_0$, $Z_2^0(\rho) = a_3(2\rho^2 - 1)$, $Z_4^0(\rho) = a_8(6\rho^4 - 6\rho^2 + 1)$ and $Z_6^0(\rho) = a_15(20\rho^6 - 30\rho^4 + 12\rho^2 - 1))$ is fitted to the OPL profile where $\rho = r/R$ [21]. The focal distance can then be calculated from a_3 while a_8 and a_{15} are indicators of the spherical aberrations present in the lens.

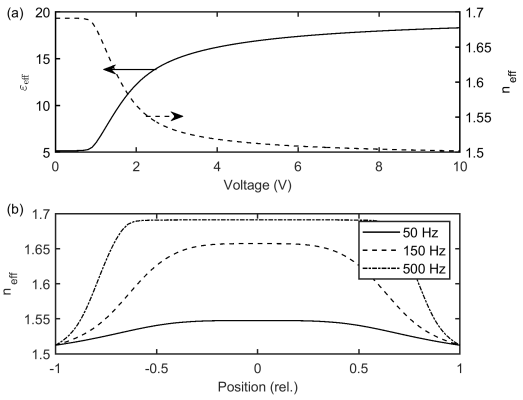

Fig. 2. (a) Variation of ε_{eff} and n_{eff} as a function of voltage. (b) Effective index profile for an applied voltage of 5 V for three different frequencies.

To look into the influence of more complex driving voltages than a simple sine function, the following algorithm is used. The driving voltage is written as a sum of sine functions each with their own amplitude and frequency. The problem is first solved for each sine with a constant ε_{eff} at each position. The root mean square value of the resulting voltages is then calculated and used to find a new value of ε_{eff} everywhere. The problem is then solved iteratively until the total solution is self-consistent.

Using a single sine function as a driving voltage results in refractive index profiles that often have a flat, almost constant part in the middle of the lens (see figure 2(b)). This is a consequence of a rather fundamental problem which is evident in the analytical solution. The first, second and third order derivatives of the Bessel functions are zero in the origin which insures a rather flat part in the middle. This results in high amounts of aberrations or weakly refracting lenses, which can be partly remedied by using a driving voltage that consists of multiple frequencies. Using for example a high amplitude low frequency sine together with a high voltage, high frequency sine (which will only influence the outside of the profile because of the high frequency) can reduce the aberrations of a strong refracting lens. In figure 3 one profile belongs to a single sine and shows the expected profile

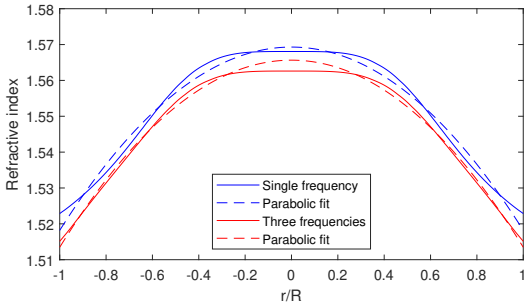

Fig. 3. Refractive index profile for a voltage of 240Hz and 5V. In the second curve two extra frequency components of 2850Hz and 6V, 80Hz and 1V are added.

oscillating above and below the parabolic fit while the other profile shows the same sine together with both a high and low frequency sine, resulting in a more parabolic profile. The correct choice of driving voltages is thus an important one.

3. MINIMIZATION OF LENS ABERRATIONS

A large case study simulation is performed to find the optimal driving voltages for different focal lengths. Optimal in this case means that the fitted Zernike polynomials are a reasonable fit and the spherical aberrations are minimal (the sum of a_8 and a_{15} is minimal) while the theoretical focal length stays within a 5% margin. Two specific additional frequency components proved useful in reducing the overall aberrations. First using a high frequency high amplitude sine such as described above to influence the outer rim of the profile and second using a low frequency sine with an RMS amplitude around 1 V to insure the voltage never drops underneath 1 V where the refractive index would remain constant. In figure 4 the optical power and spherical aberrations are plotted for some different single frequencies. In the same figure are the results for some well-chosen combinations of frequencies. It is clear that they show less aberrations for their individual optical powers than the single frequencies.

4. DEVICE FABRICATION

A LC tunable lens is fabricated starting from two ITO coated substrates (70 to 100 Ω/sq). On one substrate, the ITO was etched away in circular patterns with different radii. This substrate was

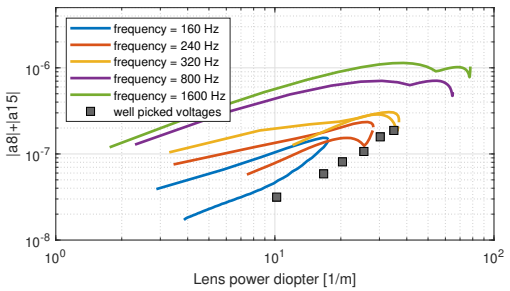

Fig. 4. Aberrations of LC lenses driven with a single frequency compared to multiple frequency driving. This is a lens with radius 250 μm and a LC layer thickness of 20 μm and a sheet resistivity of 20 GΩ/sq.

Table 1. Measured sheet resistivity of amorphous Ge films.

Thickness (nm)	Sheet resistance (Ω/sq)
5 nm	5.50×10^{11}
10 nm	8.49×10^{10}
20 nm	3.00×10^{10}

subsequently coated with amorphous Ge using e-gun evaporation. Initially, high resistivity PEDOT:PSS was used for the weakly conductive electrodes as reported in [22], but it became clear that the resistivity of the PEDOT:PSS was not stable. After a few days, conductivity of the layers reduced to zero. For that reason we opted for thin layers of amorphous Ge because they are able to provide the high sheet resistivity needed for the weakly conductive layer. Layers with different Ge thickness were evaporated and tested for their sheet resistance of which the results are listed in table 1. This value remained nearly constant over the course of days in contrast to the PEDOT:PSS layers. A drawback of using the Ge layers is a low transmission and hence introduces the restriction to reflective tunable lenses. In the remaining of this work, the fabricated lenses are analyzed in transmission. In reflection, the focal strength of the lenses is double because the light passes twice through the LC layer. The experimental results presented here are for the 20 nm thick Ge layer. Both substrates are consequently coated with an alignment layer (nylon) and rubbed. Both substrates are assembled with antiparallel alignment using 13 μm spacers dissolved in UV curable glue. The cell was then capillary filled with the LC E7 from Merck.

5. EXPERIMENTAL RESULTS

A LC lens with a diameter of 700 μm is analyzed using a polarization microscope. The device is put under crossed polarizers with the rubbing direction at 45° with respect to the polarizers. The recorded transmission in figure 5 gives an indication of the local retardation inside the ring with low sheet conductivity. The retardation is in turn a good indication of the OPL. In figure 5(a) the driving voltage signal consists of one sinusoidal component of 500 Hz and 3 V. Adding another sinusoidal component at 3000 Hz and 5 V does not change the retardation near the center of the region, but only influences the retardation in the outer region. This can also been seen from figure 5(c) which presents the extracted refractive index profiles from the microscope pictures. Figure 5(d) shows the simulated transmission for the same parameters as in figure 5(b). It is clear that there is a strong resemblance between the simulated and experimental transmission between crossed polarizers, indicating the validity of the simulation model.

Next, an experiment was set up to test the focusing properties of the lens. An LED lamp, followed by a linear polarizer, was put at a large distance of the LC lens. A CMOS camera was then put in the expected focal plane of the lens and the resulting images are shown in figure 6. When the LC lens is inactive (no voltage applied), no noticable light is observed in the focal plane. With a single frequency sinusoidal applied voltage of 3 V and 500 Hz a ring-shaped intensity pattern can be observed (see figure 6(a)). By adding a second higher frequency component to the signal, one of the rings of light in the original pattern is focused onto a relatively small point as shown in figure 6(b) and (c). When

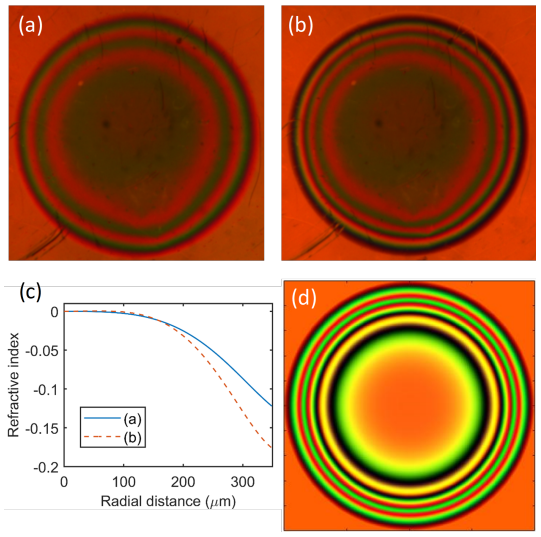

Fig. 5. (a) & (b) Polarizing optical microscope images of a 700 µm diameter lens. (a) has an applied voltage of 500 Hz and 3 V while (b) has a second component added of 3000 Hz and 5 V. (c) Extracted refractive index profile from the microscope images. (d) Artificially created image based on numerical simulations of the device with the same driving voltage as in (b).

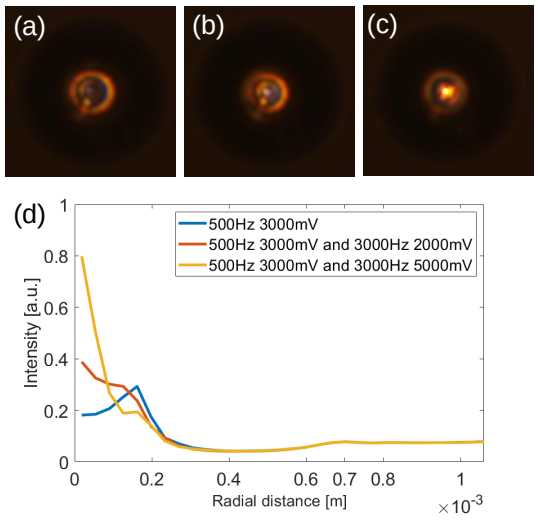

Fig. 6. Images of an LED light source through the LC lens of figure 5. (a) has an applied voltage of 500 Hz and 3 V. (b) has a second component added of 3000 Hz at 2 V and (c) an added component of 3000 Hz and 5 V. (d) Radial intensity profile extracted from the images in (a), (b) and (c).

performing the experiments, it became clear that the area of almost constant refractive index in the middle of the lens causes aberrations that cannot be avoided. It is the light coming from the edge of the lens that is much better focused when adding additional frequency components. The light passing through the middle is barely influenced. The radial intensity profile for different amplitudes of the high frequency component are visible in figure 6(d). It is clear that an additional frequency component offers a large improvement in the optical power that is located in the focal spot.

6. CONCLUSIONS

In this paper we show, both through simulations based on a theoretical model as experimentally, that the refractive index profile of a tunable lens based on a weakly conducting layer with one single electrode can be changed to reduce the aberrations by employing a voltage signal with multiple frequency components. The weakly conducting layer of germanium is shown to have appropriate sheet resistivity for lenses with radii of several hundreds of microns. A remaining issue with these lens designs however is the fact that the center region is hardly influenced by higher frequency components which leaves the lens aberrations in the middle unchanged. More complex lens designs, such as the use of an inner floating ring [18] might resolve this remaining issue.

Funding. Tom Vanackere is funded by the Research Foundation-Flanders (FWO) as PhD Fellow under grant nr. 11F5320N.

Disclosures. The authors declare no conflicts of interest.

REFERENCES

1. P. F. McManamon, P. J. Bos, M. J. Escuti, J. Heikenfeld, S. Serati, H. Xie, and E. A. Watson, Proc. IEEE **97**, 1078 (2009).
2. J. Beeckman, K. Neyts, and P. Vanbrabant, Opt. Eng. **50**, 081202 (2011).
3. I. Moreno, J. A. Davis, T. M. Hernandez, D. M. Cottrell, and D. Sand, Opt. Express **20**, 364 (2012).
4. C. Maurer, A. Jesacher, S. Bernet, and M. Ritsch-Marte, Laser & Photonics Rev. **5**, 81 (2011).
5. Y.-H. Lin, Y.-J. Wang, and V. Reshetnyak, Liq. Cryst. Rev. **5**, 111 (2017).
6. O. Sova, V. Reshetnyak, T. Galstian, and K. Asatryan, J. Opt. Soc. Am. A **32**, 803 (2015).
7. L. W. Li, D. Bryant, T. Van Heugten, and P. J. Bos, Opt. Express **21**, 8371 (2013).
8. O. Willekens, J. P. George, K. Neyts, and J. Beeckman, Opt. Express **24**, 8088 (2016).
9. J. Beeckman, T.-H. Yang, I. Nys, J. P. George, T.-H. Lin, and K. Neyts, Opt. Lett. **43**, 271 (2018).
10. M. Ye, B. Wang, and S. Sato, Opt. Express **16**, 4302 (2008).
11. N. Fraval and J. L. D. de la Tocnaye, Appl. Opt. **49**, 2778 (2010).
12. N. Fraval, F. Berier, and O. Castany, Moems Miniaturized Syst. XI **8252**, 82520Q (2012).
13. F. Chu, L.-L. Tian, R. Li, X.-Q. Gu, X.-Y. Zhou, D. Wang, and Q.-H. Wang, Liq. Cryst. **0**, 1 (2019).
14. H. D. Vleeschouwer, A. Verschueren, F. Bougrioua, R. van Asselt, E. Alexander, S. Vermael, K. Neyts, and H. Pauwels, Jpn. J. Appl. Phys. **40**, 3272 (2001).
15. K. Neyts and F. Beunis, *Ion Transport in Liquid Crystals* (Wiley-VCH Verlag GmbH & Co. KGaA, 2014), chap. 11.
16. J. Beeckman, I. Nys, O. Willekens, and K. Neyts, J. Appl. Phys. **121** (2017).
17. C.-J. Hsu, J.-J. Jhang, and C.-Y. Huang, Opt. Express **24**, 16722 (2016).
18. Y. Hsu, B. Chen, and C. Sheu, IEEE Photonics Technol. Lett. pp. 1–1 (2019).
19. T. Galstian, K. Asatryan, V. Presniakov, A. Zohrabyan, A. Tork, A. Bagramyan, S. Careau, M. Thiboutot, and M. Cotovanu, Opt. Lett. **41**, 3265 (2016).
20. C.-J. Hsu, J.-J. Jhang, J.-C. Jhang, and C.-Y. Huang, Liq. Cryst. **45**, 40 (2018).
21. H. Gross, H. Zğge, M. Peschka, and F. Blechinger, *Aberrations*, pp. 1—70. in *Handbook of Optical Systems* Edited by Herbert Gross Volume 3: Aberration Theory and Correction of Optical Systems; (Wiley-VCH Verlag GmbH & Co. KGaA, 2006)
22. X. Shang, A. M. Trinidad, P. Joshi, J. D. Smet, D. Cuypers, and H. D. Smet, IEEE Photonics J. **8**, 1 (2016).

REFERENCES

1. P. F. McManamon, P. J. Bos, M. J. Escuti, J. Heikenfeld, S. Serati, H. Xie, and E. A. Watson, "A review of phased array steering for narrow-band electrooptical systems," Proc. IEEE **97**, 1078–1096 (2009).
2. J. Beeckman, K. Neyts, and P. Vanbrabant, "Liquid-crystal photonic applications," Opt. Eng. **50**, 081202 (2011).
3. I. Moreno, J. A. Davis, T. M. Hernandez, D. M. Cottrell, and D. Sand, "Complete polarization control of light from a liquid crystal spatial light modulator," Opt. Express **20**, 364–376 (2012).
4. C. Maurer, A. Jesacher, S. Bernet, and M. Ritsch-Marte, "What spatial light modulators can do for optical microscopy," Laser & Photonics Rev. **5**, 81–101 (2011).
5. Y.-H. Lin, Y.-J. Wang, and V. Reshetnyak, "Liquid crystal lenses with tunable focal length," Liq. Cryst. Rev. **5**, 111–143 (2017).
6. O. Sova, V. Reshetnyak, T. Galstian, and K. Asatryan, "Electrically variable liquid crystal lens based on the dielectric dividing principle," J. Opt. Soc. Am. A **32**, 803–808 (2015).
7. L. W. Li, D. Bryant, T. Van Heugten, and P. J. Bos, "Near-diffraction-limited and low-haze electro-optical tunable liquid crystal lens with floating electrodes," Opt. Express **21**, 8371–8381 (2013).
8. O. Willekens, J. P. George, K. Neyts, and J. Beeckman, "Ferroelectric thin films with liquid crystal for gradient index applications," Opt. Express **24**, 8088–8096 (2016).
9. J. Beeckman, T.-H. Yang, I. Nys, J. P. George, T.-H. Lin, and K. Neyts, "Multi-electrode tunable liquid crystal lenses with one lithography step," Opt. Lett. **43**, 271–274 (2018).
10. M. Ye, B. Wang, and S. Sato, "Realization of liquid crystal lens of large aperture and low driving voltages using thin layer of weakly conductive material," Opt. Express **16**, 4302–4308 (2008).
11. N. Fraval and J. L. D. de la Tocnaye, "Low aberrations symmetrical adaptive modal liquid crystal lens with short focal lengths," Appl. Opt. **49**, 2778–2783 (2010).
12. N. Fraval, F. Berier, and O. Castany, "Novel resistive electrode structure for liquid crystal modal lens shifting," Moems Miniaturized Syst. XI **8252**, 82520Q (2012).
13. F. Chu, L.-L. Tian, R. Li, X.-Q. Gu, X.-Y. Zhou, D. Wang, and Q.-H. Wang, "Adaptive nematic liquid crystal lens array with resistive layer," Liq. Cryst. **0**, 1–9 (2019).
14. H. D. Vleeschouwer, A. Verschueren, F. Bougrioua, R. van Asselt, E. Alexander, S. Vermael, K. Neyts, and H. Pauwels, "Long-term ion transport in nematic liquid crystal displays," Jpn. J. Appl. Phys. **40**, 3272–3276 (2001).
15. K. Neyts and F. Beunis, *Ion Transport in Liquid Crystals* (Wiley-VCH Verlag GmbH & Co. KGaA, 2014), chap. 11.
16. J. Beeckman, I. Nys, O. Willekens, and K. Neyts, "Optimization of liquid crystal devices based on weakly conductive layers for lensing and beam steering," J. Appl. Phys. **121** (2017).
17. C.-J. Hsu, J.-J. Jhang, and C.-Y. Huang, "Large aperture liquid crystal lens with an imbedded floating ring electrode," Opt. Express **24**, 16722–16731 (2016).
18. Y. Hsu, B. Chen, and C. Sheu, "Improvement of hole-patterned electrode liquid crystal lens by coplanar inner ring electrode," IEEE Photonics Technol. Lett. pp. 1–1 (2019).
19. T. Galstian, K. Asatryan, V. Presniakov, A. Zohrabyan, A. Tork, A. Bagramyan, S. Careau, M. Thiboutot, and M. Cotovanu, "High optical quality electrically variable liquid crystal lens using an additional floating electrode," Opt. Lett. **41**, 3265–3268 (2016).
20. C.-J. Hsu, J.-J. Jhang, J.-C. Jhang, and C.-Y. Huang, "Influence of floating-ring-electrode on large-aperture liquid crystal lens," Liq. Cryst. **45**, 40–48 (2018).
21. H. Gross, H. Zğge, M. Peschka, and F. Blechinger, *Aberrations*, pp. 1—70. in *Handbook of Optical Systems* Edited by Herbert Gross Volume 3: Aberration Theory and Correction of Optical Systems; (Wiley-VCH Verlag GmbH & Co. KGaA, 2006)
22. X. Shang, A. M. Trinidad, P. Joshi, J. D. Smet, D. Cuypers, and H. D. Smet, "Tunable optical beam deflection via liquid crystal gradient refractive index generated by highly resistive polymer film," IEEE Photonics J. **8**, 1–11 (2016).